Overview of the Fermilab muon g-2 experiment

SeungCheon Kim (for the muon g-2 Collaboration)

Cornell University, Ithaca, NY, 14853, USA

Abstract: The measurement of the anomalous magnetic moment of muon provides a precision test of the Standard Model. The Brookhaven muon g-2 experiment (E821) measured the muon magnetic moment anomaly with 0.54 ppm precision, a more than 3 σ deviation from the Standard Model predictions, spurring speculation about the possibility of new physics. The new g-2 experiment at Fermilab (E989) will reduce the combined statistical and systematic error of the BNL experiment by a factor of 4. An overview of the new experiment is described in this article.

Key words: muon, anomalous magnetic moment

PACS: 14.60.Ef, 13.40.Em

1 Introduction

The muon anomaly (a_μ) is defined as $a_\mu = (g_\mu - 2)/2$, which refers to the term incorporating all the corrections to the Dirac magnetic moment ($g_\mu = 2$). The precise measurement of a_μ has been pursued for many decades since the early measurements in 1960s at Nevis [1] and CERN [2]. A graph of the history of the measurement precision is seen in Fig. 1 with the corresponding uncertainty and the relevant physics associated with the decreasing uncertainty. The latest measurement (E821) was conducted at Brookhaven National Laboratory (BNL) and was reported with an uncertainty of 0.54 ppm in 2004 [4, 5]. This uncertainty is already one third of the electro-weak contribution so that it has the sensitivity to check all major Standard Model (SM) contributions.

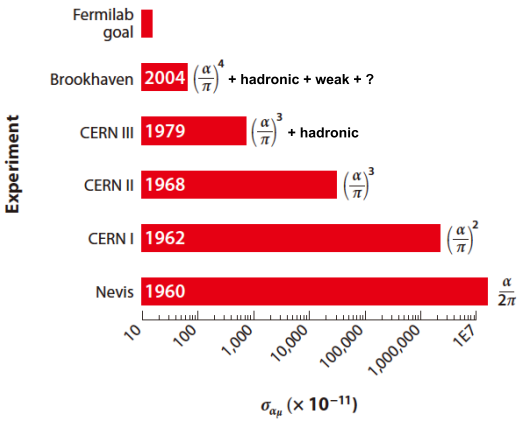

Fig. 1. The history of the a_μ measurement with the uncertainty and the physics reach as the uncertainty decreased [3].

Table 1 summarizes the various SM contributions and theoretical errors, as well as the experimental value.

Table 1. Summary of a_μ measurement and Standard Model prediction. Two values are quoted because of the two recent evaluations of the lowest order hadronic vacuum polarization.

	VALUE ($\times 10^{-11}$) UNITS
QED [6]	116 584 718.951 $\pm$ 0.009 $\pm$ 0.019 $\pm$ 0.007 $\pm$ 0.077
HVP(lo) [7]	6 923 $\pm$ 42
HVP(lo) [8]	6 949 $\pm$ 43
HVP(ho) [8]	-98.4 ± 0.7
HLbL [10]	105 ± 26
EW [11]	153.6 ± 1.0
Total SM [7]	116 951 802 $\pm$ 42 $\pm$ 26 $\pm$ 2($\pm 49_{\rm tot}$)
Total SM [8]	116 951 828 $\pm$ 43 $\pm$ 26 $\pm$ 2($\pm 50_{\rm tot}$)
Exp [5]	116 592 089 $\pm$ 63
Δa_μ(Exp - SM)	287 $\pm$ 80 [7]
	261 $\pm$ 80 [8]

The interesting thing is as one can see at the bottom of the table, the latest measurement shows $3.3-3.6\sigma$ deviation from the SM prediction. As this discrepancy can imply the emergence of the new physics beyond the SM, the efforts to improve the precision of the knowledge of a_μ have been pushed in both theoretical and experimental sides. The muon g-2 experiment at Fermilab (E989) is a follow-up experiment of E821 at BNL mainly motivated by this discrepancy. The goal of the new experiment is to reduce the uncertainty to 0.14 ppm, which is one fourth of the previous experimental error. For this goal, the experiment is aiming at reducing the statistical uncertainty from 0.46 ppm to 0.10 ppm by increasing the muon beam intensity and beam repetition rate and improving the muon capture efficiency. The systematic uncertainty is also expected to be reduced to 0.1 ppm based on the upgrade of the experimental techniques [9].

1) E-mail: sk2528@cornell.edu

2 The basic principle of the experiment

The basic principle of the experiment is to observe the precession of the spin of the polarized muon relative to its momentum in the uniform magnetic field. In the uniform magnetic field, the muon particle will have a cyclotron motion and the muon spin will precess relative to its momentum with a certain angular frequency, which is called ω_a. For the uniform magnetic field environment, the storage ring magnet with electrostatic vertical focusing will be used. In the presence of the electric field $\vec{E}$, ω_a is determined by the following equation assuming the momentum is transverse to the magnetic field.

$$\vec{\omega}_a = -\frac{e}{m_\mu}\left[a_\mu \vec{B} - \left(a_\mu - \left(\frac{m_\mu c}{p_\mu}\right)^2\right)\frac{\vec{\beta}\times\vec{E}}{c}\right]. \quad (1)$$

If p_μ is chosen as 3.094 GeV/c, the second term in Eq. 1 vanishes so that $\vec{\omega}_a$ solely depends on a_μ and the magnetic field according to the following equation.

$$\vec{\omega}_a = -\frac{e}{m_\mu} a_\mu \vec{B}. \quad (2)$$

From this equation, one can see that given $\vec{B}$, non-zero a_μ leads to the non-zero angular frequency. Figure 2 illustrates the precession according to different values of g_μ.

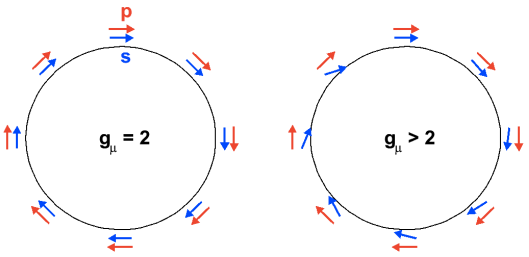

Fig. 2. An illustration of the spin precession relative to the momentum in the uniform magnetic field by g_μ.

The muon spin orientation can be observed by measuring the energy and arrival time of the high energy positron from muon decay with the calorimeters. Thanks to the parity violation of muon decay, the high energy positrons in the muon rest frame are preferentially emitted parallel to the spin orientation. Figure 3(a) shows the distribution of the positron emission angle (relative to the spin) and its energy in the muon rest frame. In the lab frame, the positron energy spectrum varies by the spin orientation with respect to the momentum as seen in the Fig. 3(b). Therefore, the spin precession leads to the positron energy dependent event rate modulation at the calorimeters. Figure 4 shows the event rate modulation at the calorimeters for positrons whose detected energy is above the threshold energy, 1.8 GeV.

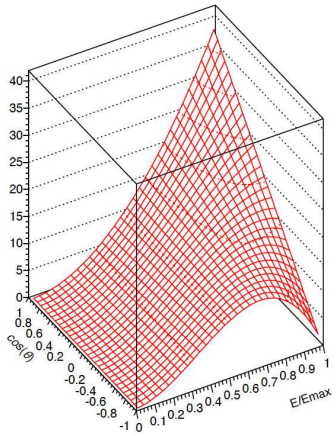

(a)

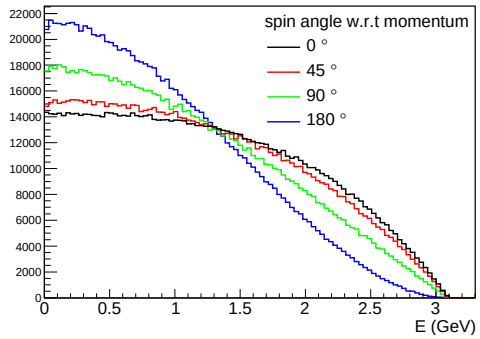

(b)

Fig. 3. (a) The distribution of the positron emission angle relative to the spin and its energy at the muon rest frame. (b) The positron energy spectrum by the spin orientation with respect to the momentum at the lab frame.

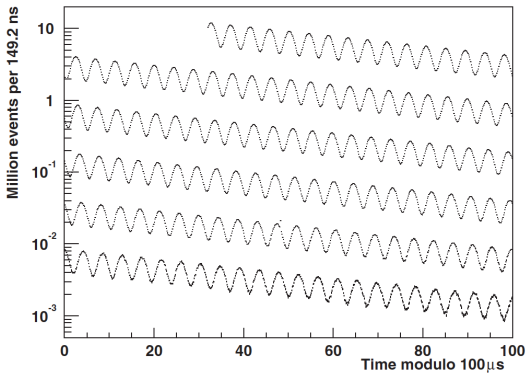

Fig. 4. The modulation of the positron event rate at the calorimeters displayed with 100 μs modulo [5].

By fitting this event rate modulation, one can obtain the ω_a frequency. Recalling Eq. 2, to measure the a_μ, magnetic field B needs to be known as well. To minimize variation of the muon precession frequency over the storage volume, uniformity of the magnetic field is essential.

Since the muon storage ring magnet which was used in E821 experiment proved to be sufficiently uniform, this same storage ring magnet will be used for the new experiment (Fig. 5). For the determination of a_μ at 140 ppb level, the magnetic field will be determined to 70 ppb using nuclear magnetic resonance (NMR).

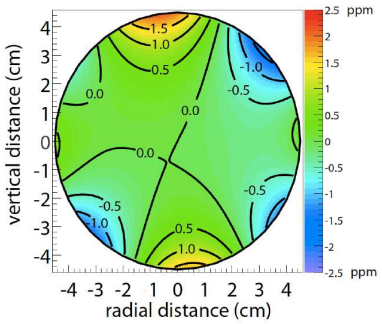

Fig. 5. A contour plot of the magnetic field averaged over azimuth of the ring at 0.5 ppm intervals.

The magnetic field in the muon storage region will be expressed in terms of the proton Larmor frequency ω_p as $\hbar\omega_p = 2\mu_p|B|$, where μ_p is the proton magnetic moment. With measured ω_a and ω_p, one can obtain a_μ using the following relation based on Eq. 2.

$$a_\mu = \frac{\omega_a}{\omega_p}\frac{2\mu_p}{\hbar}\frac{m_\mu}{e} = \frac{\omega_a}{\omega_p}\frac{\mu_p}{\mu_e}\frac{m_\mu}{m_e}\frac{g_e}{2}. \quad (3)$$

where μ_e is the electron magnetic moment, m_e electron mass and g_e electron g-factor. The values for μ_e/μ_p and m_μ/m_e are taken from other independent muonium hyperfine structure experiment [12] to determine a_μ at the best precision. Currently, μ_e/μ_p is measured to be $-658.210\ 6848(54)$ with 8.1 ppb uncertainty and m_μ/m_e $206.768\ 2843(52)$ with 25 ppb uncertainty. $g_e/2$ is measured independently to be $1.001\ 159\ 652\ 180\ 73(28)$ (0.28 ppt uncertainty) [12, 13].

3 Overview of the experimental technique

3.1 Muon beam production

The muon g-2 experiment will take advantage of the infrastructure of the former antiproton source at Fermilab. Figure 6(a) shows the Fermilab accelerator complex for muon beam production. The Booster will accelerate protons up to 8 GeV and send them to the Recycler ring. The proton beam will be re-bunched in the Recycler ring into four beam bunches and transported to a target constructed of a solid Inconel 600 core. Upon hitting the target with the proton beams, the secondary π^+ particles with a momentum of 3.11 GeV/c ($\pm$ 10 %) will be collected. The secondary beam will travel through transfer lines which are designed to capture as many muons with momentum 3.094 GeV/c from pion decay as possible. Since μ^+ from π^+ decay is always left-handed in the π^+ rest frame and the high momentum muons in the lab frame are from the pion decay in the forward direction, the high energy muon beam is highly polarized. The beam will be injected in the delivery ring and during several revolutions around the delivery ring, the muons will be separated in time from the heavier residual protons and the proton contamination will be aborted with a kicker. The pure muon beam will be extracted into the beam transfer lines which leads to the muon g-2 storage ring magnet.

(a)

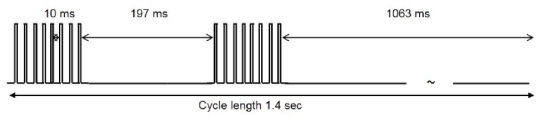

(b)

Fig. 6. (a) The bird's eye view of the Fermilab acceleratory complex for muon beam production. (b) Possible time structure of beam pulses for the experiment.

While not finalized, one scenario to fill the ring magnet has the time structure in Fig. 6(b), which leads to a 12 Hz average fill rate. In this scenario, one cycle of the beam is 1.4 second and there are two groups of beam bunches in one cycle. The two groups are separated by 197 ms and in each group there are 8 beam bunches arriving in 10 ms intervals. For one beam bunch, initially, 10^{12} protons will be supplied to the target and about 8.1×10^5 muons will be delivered to the muon storage ring and evetually, about 10^4 muons will be stored in the ring.

3.2 The muon storage ring magnet

The storage ring magnet which was used in E821 experiment will be reused in the new experiment, since the ring magnet proved its 1 ppm level uniformity at the cross section of the muon storage region (Fig. 5) and 100 ppm variation along the cicumference. The ring magnet is a superferric magnet. The field of the magnet is 1.451 T and the required current is 5200 A. The radius of the equilibrium orbit is 7.112 m and the diameter of the muon storage region is 90 mm. Figure 7(a) shows the details of the cross section of the ring magnet. The 15 meter diameter superconducting coils were transported from Brookhaven to the new experimental hall at Fermilab in the summer of 2013 by Emmert International logstics company [14], which took 3200 miles over land and sea for 35 days. After reassembling the ring magnet and repairing some minor issues, the ring magnet demonstrated its full magnetic field of 1.45 T in September 2015.

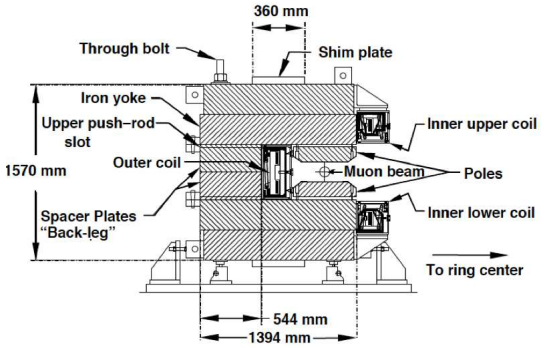

(a)

(b)

Fig. 7. (a) The cross section of the muon storage ring magnet. (b) The ring magnet moved into the new experimental hall at Fermilab.

3.3 Injecting muon beam into the storage ring

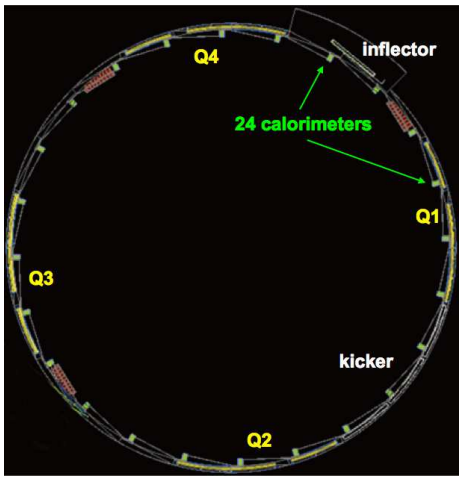

Fig. 8. The layout of the muon storage ring and the placement of other equipments. Q1-4 are quadrupoles placed with 4 fold symmetry.

The muon beam will be injected through a hole in the back leg iron and into the gap of the dipole. The inflector is a superconducting magnet that isolates the injected muons from the dipole field so that the muon trajectory is tangential to the closed orbit of the storage ring. Since the inflector exit is 77mm away from the ring orbit center, the orbit of the injected muons is displaced from the nominal orbit of the ring. To guide the muon particles onto the stable orbit, the injected muons are pushed into the stable orbit by the kicker. The injected muons cross the central orbit at 10.8 mrad at 90 degree azimuthal position with respect to the inflector exit. The 10.8 mrad kick, corresponding to an integrated field of 1.1 kG-m, is provided by the pulsed kicker magnet. The kicker system consists of 3 independent 1.27 m long magnets. The ideal kicker pulse has fast rise and fall time and width greater than 120 ns but smaller than one revolution period of 149 ns to avoid multiple kicks. The kicker system is very important because it influences the muon storage efficiency and the amplitude of coherent betatron oscillation. The kicker system was designed with the double transmission line (Blumlein pulse forming network) made of 3 concentric cylinder. The kicker magnet is a pair of parallel aluminum plates which have arc shape for the efficient magnetic field generation for a given current through the plates. The required peak magnetic pulse is 292 Gauss and for this magnetic field, about 4.5 kA current is supplied to the kicker magnet. Figure 9(a) shows the prototype kicker system built at Cornell University and the resulting kicker pulse profile is shown in Fig. 9(b).

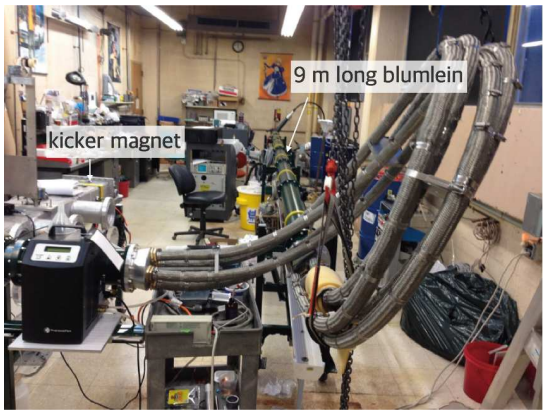

(a)

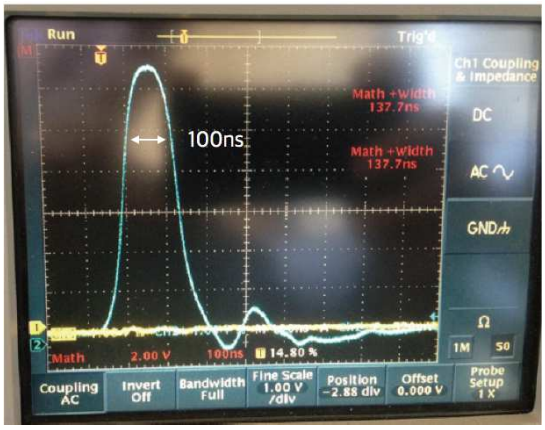

(b)

Fig. 9. (a) The prototype kicker system built at Cornell University. (b) The kicker pulse profile from the prototype kicker system.

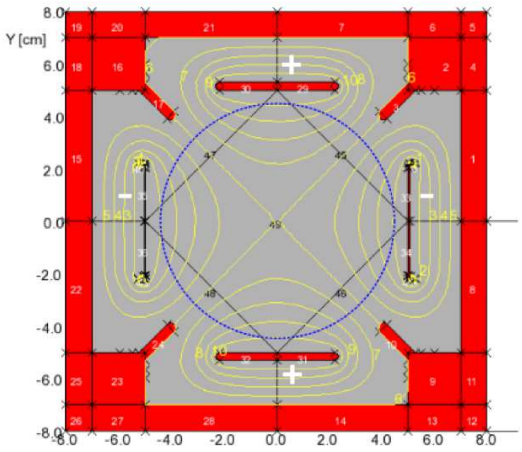

Fig. 10. An opera model of electrostatic quadrupole.

3.4 Storing the muon beam in the storage ring

To confine muons vertically in the uniform magnetic field, electrostatic quadrupoles will be used to provide the vertical focusing. The quadrupoles are divided into 4 sections (Q1-4) with 4 fold symmetry (Fig. 8). Figure 10 shows the cross section view of the quadrupole and associated electric field simulated by Opera software [15]. The betatron frequencies are determined by the quadrupole voltage. Since the muon beam passes each calorimeter with a cyclotron frequency(f_C), the betatron frequency (f_x) observed by one calorimeter is f_{CBO}, which is the difference between f_C and f_x. In the E821 experiment, f_{CBO} is close to double the ω_a precession frequency so that it disturbed the exact determination of ω_a. In the new experiment, the strength of the quadrupole will be increased to significantly reduce the effect of f_{CBO} on the ω_a determination.

3.5 Detecting positrons from muon decay

The decay positrons will be detected at the calorimeters mounted along the inner radius of the vacuum chamber in the ring magnet. There will be 24 calorimeter stations located with 15 degree interval azimuthally(Fig. 8). The calorimeter will measure the positron energy and arrival time. For the calorimeter, lead fluoride(PbF_2) crystal will be used because it has fast Cherenkov signal response and good energy resolution. For the photon detection, silicon photomultipliers (SiPM) will be used since they have high photon-detection efficiency, fast time response and they do not perturb the magnetic field of the storage ring [16]. The signal will be digitized with a waveform digitizer with 12 bit resolution at 800 Msps. Figure 11 shows an array of PbF_2 crystals for a beam test conducted at SLAC in Spring 2015.

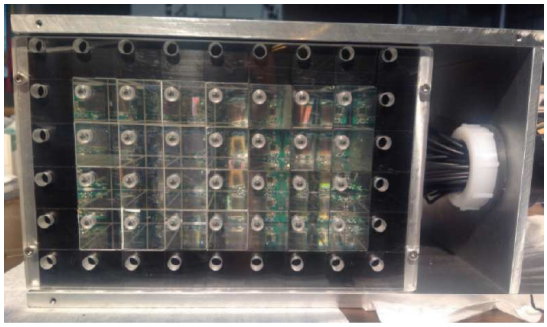

Fig. 11. PbF_2 crystal array for a beam test.

One of the important issues related to the calorimeter is pile-up events. If two low energy events hit a calorimeter at the same time, this event can be misidentifed as a high energy event. The high energy positron travels a longer distance to hit the calorimeter because the smaller curvature of the positron orbit compared to low energy positrons. If the low energy events are misidentified as one high energy event, it can distort the phase of the event rate modulation. The pile-up rate decreases exponentially with half the life time of muon decay. Therefore, the time dependent phase shift of the event rate

modulation can alter the measurement of ω_a. In the E821 experiment, the systematic error from the pile-up events was estimated to be 80 ppb. In the new experiment, one calorimeter station will be composed of a 6×9 array of crystals in which one crystal is 25×25×140 mm^3. This array design will have about 4-5 fold pile-up event reduction compared to the E821 monolithic calorimeter. Also, thanks to the fast time response of the calorimeter, events that occur with a time interval larger than 3 ns interval can be reliably separated (Fig. 12).

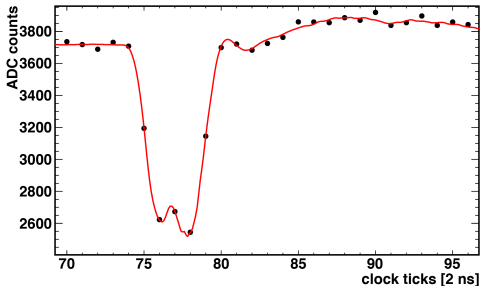

Fig. 12. A signal from a SiPM bench test with a preliminary pulse shape. Shown here are two independent pulses with a 3 ns time separation.

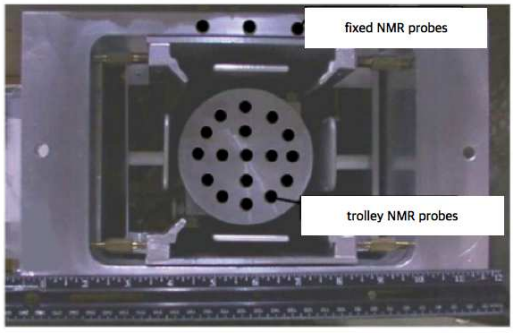

Fig. 13. The E821 NMR probe trolley in the vacuum chamber.

3.6 Measuring the magnetic field in the muon storage region

The magnetic field in the muon storage region will be measured with proton NMR as in the E821 experiment. The NMR probes will utilize protons in samples of petroleum jelly. There will be 378 NMR probes around the muon storage region to constantly monitor the magnetic field to a precision of 20 ppb and stablize the field while muons are stored. The magnetic field in the muon storage region will be mapped with 17 NMR probes carried by the trolley using routine break time for the trolley run. The trolley measurement will be conducted at 6000 azimuthal locations inside the muon storage ring. During this trolley run, the monitoring NMR probe will be cross calibrated with the trolley NMR probes. Eventually, the external NMR probe measurement will be translated into the free proton Larmor frequency with an accuracy of 35 ppb through an absolute calibration. Figure 13 shows the E821 NMR trolley in the vacuum chamber, where muon particles are stored. During the data collection time, the trolley is moved into the garage and during the break, the trolley will scan the storage ring moving on the rail mounted on the vacuum chamber. The figure also shows the location of the fixed monitoring NMR probes.

4 Conclusion

The precision calculation and measurement of the muon magnetic moment anomaly a_μ is an important low energy test of the Standard Model. Currently, the precision of the measurement is 0.54 ppm and the new Fermilab g-2 experiment is aiming at reducing the uncertainty to 0.14 ppm with the increased muon particle delivery and storage and improved experimental technique to reduce the systematic error by more than a factor of two compared to the BNL measurement. If the central values of the new measurement and the theoretical prediction remain unchanged, the discrepancy between the measurement and the prediction will have a significance of 5σ. As it is also expected that the theoretical uncertainty will be reduced to 0.2 ppm level in next years, the significance can be as high as 8σ. Now, the detailed design of the experiment is almost complete and most of the parts are already under construction. After commissioning, the first data taking is expected to start in 2017.

References

1 R.L. Garwin, et al. Phys. Rev. 1960,118:271 .
2 G. Charpak et al., Phys. Rev. Lett. 1961,6:128; Nuovo Cim. 1961, 22:1043; Phys. Lett. 1962, 1:16; Nuovo Cim. 1965, 37:1241
3 J.P. Miller, et al., Annu. Rev. Part. Sci. 2012, 62:237
4 G. Bennett, et al., (Muon (g-2) collaboration) Phys. Rev. Lett. 2004, 92:161802
5 G. Bennett, et al., (Muon (g-2) collaboration) Phys. Rev. D 2006, 73:072003
6 T. Aoyama, et al., Phys. Rev. Lett. 2012, 109:111808
7 M. Davier, et al., Eur. Phys. J. C 2011, 71:1515
8 K. Hagiwara, et al., J. Phys. G 2011, 38:085003
9 J. Grange, et al., (muon g-2 (E989) collaboration), Muon (g-2) Technical Design Report, 2015, arXiv:1501.06858 [physics.ins-det]
10 J. Prades, E. de Rafael and A. Vainshtein, in Advanced Series on Directions in High Energy Physics - Vol. 20 Lepton Dipole Moments, Ed. B.L. Roberts and W.J. Marciano, World Scientific, 2010, p. 303; and arXiv:0901.0306v1[hep-ph]
11 C. Gnendiger, et al., Phys. Rev. D 2013, 88:053005
12 P.J. Mohr, et al., Rev. Mod. Phys. 2012, 84:1527
13 D. Hanneke, et al., Phys. Rev. A 2011, 83:052122
14 Emmert International, 11811 SE Highway 212, Clackamas, OR 97015
15 Opera Simulation Software, COBHAM, www.operafea.com
16 A. Fienberg, et al., Nucl. Instr. Meth. Phys. Res. A 2015, 783:12